

# Chapter 4

## Micro-particles in One-dimensional Confinement

In the previous chapter, we described the phenomena that are associated with using pulsed laser ablation as a tool to mechanically excite spherical, metallic micro-particles. This approach provides the basis for transferring a controlled momentum to a system of micro-particles. However, before we proceed to study the wave propagation in micro-granular systems, we need to know how the particles behave on the substrate (i.e., we need to identify the governing equations of motion). The basic motion of a macroscopic sphere on a support structure has been studied earlier, for example in [143, 144]. In the simplest models, a sphere moving in one direction is considered as a rigid body and is subjected to Coulomb friction that acts between the surface of the sphere and the supporting structure [4]. However, the complexity of the models increases significantly if the spheres are no longer assumed as rigid bodies, and if the elastic contact force, the hysteretic losses in rolling [145], the lubricated sliding friction, the deformation of the surfaces, and the shear adhesive force are also included [145]. For example, for particles moving in an asymmetric v-shaped groove, governed by gravitation and static friction, the uneven shear force exerted on the spheres by both walls can cause the spheres to rotate. As a result, models that describe the particles' motion must account for such rotation.

In most studies of macroscopic granular systems, for example [125], the granular chains are considered as a classical system of spheres moving on a guiding rail, where only the elastic contact forces between particles are included. In these cases, the interactions between particles and their supports are usually considered negligible or are only seen as contributing to dissipation in the system.

It is questionable whether the description of macro-granular systems still applies to the micro-granular system of interest for this thesis. In the rest of this chapter, we analyze the relevant types of interactions that arise when particle size is reduced. The next chapter builds on these findings, to analyze the dynamic response of a multi-particle chain and verify if the same phenomena found in macroscopic particles (e.g., solitary wave propagation) are also present at the micro-scale.

It is well known that when particle size is reduced to the micro-scale, adhesive forces such as hydrodynamic and Van der Waals interactions become more dominant [34, 103, 146]. The particles considered in our dry systems have diameters of  $\sim 300 \mu\text{m}$ , which are much larger than the diameters of 1 to  $10 \mu\text{m}$  that are usually assumed in the DMT and JKR models; however, they are also not properly “macro-scale.” No theoretical approaches are available to describe these contact regimes. However, this intermediate size range indicates that the modeling of the system should be modified to account for the presence of the support system and air drag in the system’s dynamics.

A complete first-principle model of the dynamics of micro-particles is difficult, as not enough information is available about these particles’ physical characteristics. In this chapter, we address this issue by extracting experimental parameters from the study of the motion of individual particles on their substrate (in this case a v-shaped groove). We also derive an empirical model to describe the observed particle motion. We extract the dissipation terms, including Coulomb friction, Stokes’ viscous drag force, and quadratic drag force, and analyze the trajectories of the particles moving in the groove. In addition, we also study the interaction between two particles by extracting from experiments the coefficient of restitution upon impact and the frictional constant between two particles. The goal of our initial set of experiments is to construct an empirical description of the dynamical system that can pave the way for a complete study of wave propagation in micro-granular chains and that can serve as the foundation for the analysis that is presented in the next chapters. With the experiments described in this chapter, however, it is not possible to study either the particle contact interaction potential or specific interaction/adhesion between the particles and their support in detail.

#### 4.1. Modeling the motion of a sphere in a groove

In this section, we model the rolling and sliding motion of a spherical particle in a groove. Let the particle have a radius  $R$ , mass  $m$ , and moment of inertia  $I$ . Frictional forces between a particle and the surface of a groove are proportional to the normal force between the contact with a proportional constant,  $\mu_{pg}$ . The inclined angle between the two surfaces of the v-shaped groove is  $\theta$ , where  $\theta = 70.6^\circ$  in our system.

Let the v-grooves lie in the x-z plane, with its long axis (i.e., the direction of motion of the particle) parallel to the z-direction (Fig. 4.1). Assuming the particles do not move in the x- and y-directions, we can describe the motion of the particles with four parameters, namely  $z$ ,  $v_z$ ,  $\theta_x$ , and  $\omega_x$ , where  $z$  is the z-component of the particle displacement,  $v_z$  is the velocity in the z-direction,  $\theta_x$  is the x-

component of the particle angular displacement, and  $\omega_x$  is the  $x$ -component of the angular velocity. If there is a relative motion between the surface of the particles and the groove (i.e.,  $v_z - R\omega_x \sin(\frac{\theta}{2}) \neq 0$ ), the total force and torque resulting from the frictional forces between the particles and the two surfaces of the v-groove are respectively  $f_z = -mg\mu_{pg}/\sin(\frac{\theta}{2})$  and  $\tau_x = Rmg\mu_{pg}$ . For convenience, we define  $v_a \equiv R\omega_x$ , and  $s \equiv \sin(\frac{\theta}{2})$  as a geometric factor that depends on the inclined angle of the groove. In our system  $s$  is 0.5779.

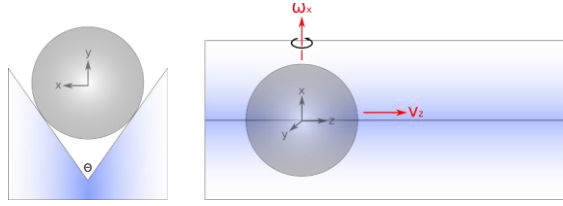


Figure 4.1: A particle in a v-shaped groove. The direction in which the particle is moving is defined as the  $z$ -direction. The particle is supported by the groove's two inclined surfaces. In comparison to when particles are placed on a flat surface, the geometry of the v-groove enhances the frictional force by a factor of  $1/\sin(\theta/2)$ , where  $\theta$  is the angle between the two surfaces of the v-groove. For the particles to roll without sliding on the groove, the groove's translational and angular velocities need to satisfy  $v_z = R\omega_x \sin(\frac{\theta}{2})$ .

We can see that when a particle is moving on the groove, the frictional force transfers energy between translational and angular motion until no relative motion occurs between the surfaces in contact:

$$v_z = sv_a. \quad (4.1)$$

When  $v_z \neq sv_a$ , the equations of motion become

$$\begin{aligned} \frac{d}{dt} v_z &= -\text{sign}(v_z - sv_a) g\mu_{pg}/s, \\ \frac{d}{dt} v_a &= \text{sign}(v_z - sv_a) kg\mu_{pg}, \end{aligned} \quad (4.2)$$

where  $\text{sign}(x)$  is the signum function with  $\text{sign}(0) = 0$ . For a particle moving in a groove, the Coulomb friction causes the particle to reach a steady state of rolling without sliding. If the system evolves from an initial state of  $v_y^{(0)}$  and  $v_a^{(0)}$  to a final steady state of  $v_y^{(1)}$  and  $v_a^{(1)}$ , the steady state velocities (defined as the velocity of the particles that are rolling without sliding) are

$$\begin{aligned}
v_z^{(1)} &= \frac{ks^2}{ks^2+1} v_z^{(0)} + \frac{s}{ks^2+1} v_a^{(0)}, \\
v_a^{(1)} &= \frac{ks}{ks^2+1} v_z^{(0)} + \frac{1}{ks^2+1} v_a^{(0)}.
\end{aligned}
\tag{4.3}$$

Starting at the initial velocities of  $v_z^{(0)}$  and  $v_a^{(0)}$ , the distance ( $\Delta z$ ) and time ( $\Delta t$ ) required to achieve steady states are, respectively,

$$\begin{aligned}
\Delta z &= \frac{1}{2} \frac{s}{ks^2+1} \frac{v_z^{(0)} - sv_a^{(0)}}{g\mu_{pg}} \left( \frac{2ks^2+1}{ks^2+1} v_z^{(0)} + \frac{s}{ks^2+1} v_a^{(0)} \right) \\
\Delta t &= \frac{s}{ks^2+1} \frac{v_z^{(0)} - sv_a^{(0)}}{g\mu_{pg}}.
\end{aligned}
\tag{4.4}$$

This means that the rolling-sliding to rolling transition happens at a time scale of  $\frac{s}{ks^2+1} \frac{v_z^{(0)}}{g\mu_{pg}}$ , which is in the order of a few milliseconds in our system. For a more realistic model of all of the physical forces that are involved in the experimental system, we include the time constant for air friction,  $T$ , which is another empirical parameter,

$$\begin{aligned}
\frac{d}{dt} v_z &= -\text{sign}(v_z - sv_a) g\mu_{pg}/s - v_z/T, \\
\frac{d}{dt} v_a &= \text{sign}(v_z - sv_a) kg\mu_{pg}.
\end{aligned}
\tag{4.5}$$

Notice that we have two dependent variables (namely  $v_z$  and  $v_a$ ) that should be investigated: we will retrieve the information for  $v_a$  through indirect fitting of the experimental data.

#### 4.2. Motion of one micro-particle in a groove

We first study the motion of a single micro-particle that is rolling in a v-shaped groove (Fig. 4.1). A micro-particle is placed in the groove and excited with the laser system (see Chapter 3) to different controlled velocities between 0 to 0.1 m/s. The particle is positioned in the groove with a computer-controlled micro-manipulator, in order to achieve accurate and repeatable initial conditions. We track the motion of a micro-particle with the optical high-speed imaging system that is described in Chapter 2. In Fig. 4.2b, we show a typical measured trajectory for a micro-particle that is moving in the groove. The particle has an initial velocity of 0.025 m/s, and from the trajectory it is evident that its motion is characterized by two different regimes: i) a rolling and sliding regime; and ii) a rolling without sliding regime (which are labeled with green and red lines, respectively). The transition time between these

two different motion regimes,  $t_1$ , as well as  $\mu_{pg}$ ,  $T$ , and the initial velocity  $v_0$  are found by fitting the experimental data numerically. The fitting parameters are obtained by minimizing the error function  $\text{Er}(\mu_{pg}, T) = \sum_n (f(t_n; v_{z0}, \mu_{pg}, T) - x_n)^2$ , where  $f(t; v_{z0}, \mu_{pg}, T)$  is the solution of Eq. (4.5),

$$f(t; \mu_{pg}, T) = \begin{cases} T \left( v_{z0} - \frac{gt\mu_{pg}}{s} + \frac{gT\mu_{pg}}{s} \right) - e^{-\frac{t}{T}} T \left( v_{z0} + \frac{gT\mu_{pg}}{s} \right), & \text{if } t < t_1 \\ e^{-\frac{t}{T}} (sv_{z0} + gT\mu_{pg} - e^{\frac{t_1}{T}} gT\mu_{pg}) / s, & \text{otherwise} \end{cases}, \quad (4.6)$$

where it is assumed the initial angular velocity is zero and  $t_1$  is the solution of  $gkst\mu_{pg} + e^{-\frac{t}{T}}(-sv_{z0} - gT\mu_{pg} + e^{t/T}gT\mu_{pg})/s = 0$ . In Figs. 4.2c-d, we plot the  $T$  and  $\mu_{pg}$  which are obtained through numerical fitting. It can be seen in Fig. 4.2c that the empirical parameter of the time constant for air friction,  $T$ , is not a constant but instead has a linear dependency on the initial velocity. The two clouds of the measured value of  $T$  obtained from the two types of particles (stainless steel 440C and stainless steel 316) overlap to give  $T = T_0 + T'v_0 = 0.052 + 1.10v_0$ . For comparison, the predicted time constant caused by the Stokes' drag in air is  $T = m/6\pi\mu R = 0.074$ . The agreement between data from particles of different materials that are the same size shows that the measured time constant is a geometric effect that is only altered by the particles' shapes and dimensions. The linear behavior of  $T$  implies that the air friction should include another correcting term that is proportional to the square of velocity:

$$\frac{v_z}{T} = \frac{v_z}{T_0 + T'v_0} \sim \frac{v_z}{T_0} - \frac{T'v_z^2}{T_0^2} \equiv \frac{v_z}{T_0} - \frac{v_z^2}{L}, \quad (4.7)$$

where  $v_z$  is the particle velocity,  $T$  is the original proposed time constant for dissipation, and  $T_0$  and  $L$  are empirical parameters that provide a more accurate representation of dissipation.

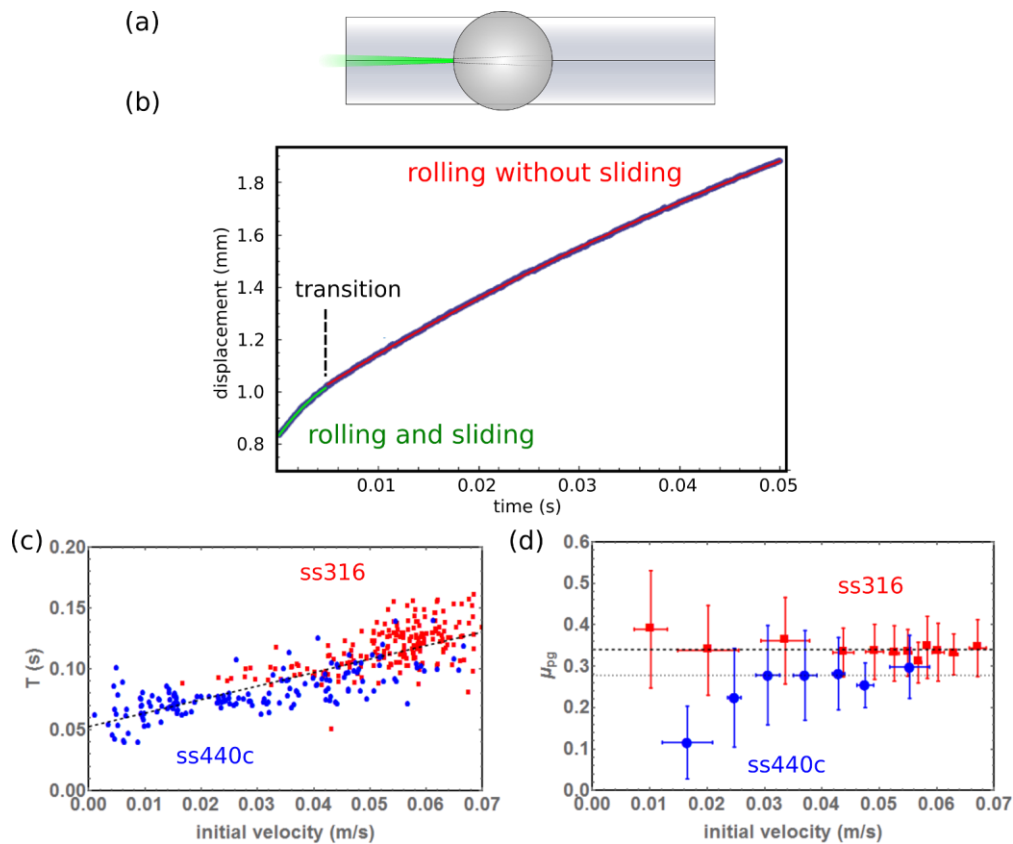


Figure 4.2: Experimental investigation of single micro-particles moving in a groove. (a) Schematic diagram of the experimental setup: a laser (green beam in the diagram) excites a particle in a groove, with a controlled pulse energy. We tested two types of micro-particles, stainless steel 316 and 440c. (b) A typical measured trajectory of an excited micro-particle. The transition from a rolling and sliding motion to rolling without sliding can be found by using an optimization algorithm to obtain the empirical parameters  $T$  and  $\mu_{pg}$ , as a function of initial velocity. (c)  $T$  is found to depend linearly on the initial velocity  $T = 0.052 + 1.10v_0$ . (d) Stainless steel 316 particles have a mean of  $\mu_{pg} = 0.337$  (dashed line) and stainless steel 440c particles have a mean of  $\mu_{pg} = 0.296$  (dotted line) for  $v_0 > 0.03 \text{ m/s}$ . The error bars are plotted with  $\pm\sigma/2$ , where  $\sigma$  is the standard deviation of the measurement.

The average friction constant,  $\mu_{pg}$ , is 0.337 for stainless steel 316 and 0.293 for stainless steel 440c particles. It can be seen that the friction coefficient for stainless steel 440c particles approaches zero at low velocity. This can result from the fact that particles made of steel 440c have much smoother surfaces and a higher quality than the steel 316 particles. The complete equations of motion for particles moving in a groove are

$$\begin{aligned}\frac{d}{dt} v_z &= -\frac{\text{sign}(v_z - sv_a)g\mu_{pg}}{s} - \left(\frac{v_z}{T_0} - \frac{v_z^2}{L}\right), \\ \frac{d}{dt} v_a &= \text{sign}(v_z - sv_a)kg\mu_{pg},\end{aligned}\tag{4.8}$$

where  $T_0 = 0.052$  s,  $L = 2.5$  mm, and  $\mu = 0.337$  and  $0.293$  for stainless steel 316 and 440c, respectively.

### 4.3. Modeling the collision of two particles in a groove

With the equations obtained in the previous section, we can move on to modeling the collision of two particles in a groove. In an ideal scenario, when two particles of the same mass collide elastically, e.g.,  $z_2 - z_1 < 2R$ , they exchange their velocity. Assuming their initial velocities are  $v_{z1}^{(1)}$  and  $v_{z2}^{(1)}$ , after an elastic collision their velocities are expected to become  $v_{z1}^{(2)} = v_{z2}^{(1)}$  and  $v_{z2}^{(2)} = v_{z1}^{(1)}$ . However, the real contact interaction between the particles is affected by the presence of a frictional force between their surfaces. If a relative sliding motion occurs between the surfaces of the two particles (i.e.,  $v_{a1} + v_{a2} \neq 0$ ), then the presence of a frictional force induces a torque at the contact and changes the angular momentum of both particles. Let  $\mu_{pp}$  be the frictional constant between the surfaces of two particles; when  $v_{a1} + v_{a2} > 0$ , we have

$$-\Delta v_{z1} = \int \frac{f}{m} dt = -\int \frac{\tau_{x1}}{m\mu_{pp}R} dt = -\frac{I\Delta\omega_{x1}}{m\mu_{pp}R} = -\frac{I\Delta v_{a1}}{m\mu_{pp}R^2}.\tag{4.9}$$

Here,  $\Delta v_z$  and  $\Delta\omega_x$  are respectively the changes in translational and angular velocity before and after the collision. In addition,  $f$  is the contact force during the impact,  $\tau_x$  is the torque resulted from the frictional force, and  $R$ ,  $m$ , and  $I$  are the radius, mass, and inertia of moment of the particle, respectively. We therefore have  $\Delta v_{a1} = \mu_{pp}k\Delta v_{y1}$  and similarly,  $\Delta v_{a2} = -\mu_{pp}k\Delta v_{y2}$ , and the resulted angular  $v_{a1}^{(2)} = R\omega_{x1}^{(2)}$ ,

$$\begin{aligned}v_{a1}^{(2)} &= v_{a1}^{(1)} + \text{sign}(v_{a1}^{(1)} + v_{a2}^{(1)})\mu_{pp}k(v_{z2}^{(1)} - v_{z1}^{(1)}), \\ v_{a2}^{(2)} &= v_{a2}^{(1)} + \text{sign}(v_{a1}^{(1)} + v_{a2}^{(1)})\mu_{pp}k(v_{z2}^{(1)} - v_{z1}^{(1)}).\end{aligned}\tag{4.10}$$

Equation (4.10) holds only when the sliding motion between the particle surfaces is not eliminated by the frictional force between the particles before the end of the impact. If the frictional force eliminates the relative motion between the surfaces during the impact, the frictional force would cease

to contribute to the change of angular velocities. In this case, we can solve the final states of angular velocities,

$$\omega_{x1}^{(2)} + \omega_{x2}^{(2)} = \frac{v_{a1}^{(2)}}{R} + \frac{v_{a2}^{(2)}}{R} = \frac{(v_{a1}^{(1)} + \Delta v_{a1})}{R} + \frac{(v_{a2}^{(1)} + \Delta v_{a2})}{R} = 0, \quad (4.11)$$

and obtain

$$\begin{aligned} v_{a1}^{(2)} &= (v_{a1}^{(1)} - v_{a2}^{(1)})/2, \\ v_{a2}^{(2)} &= (v_{a2}^{(1)} - v_{a1}^{(1)})/2. \end{aligned} \quad (4.12)$$

For the relative motion between the surfaces to be eliminated by frictional force during the impact, we require the magnitude of change in angular velocity  $|\Delta v_a|$  in Eq. (4.12) to be smaller than the one in Eq. (4.10), which translates into

$$|v_{a1}^{(1)} + v_{a2}^{(1)}| < 2\mu_{pp}k(v_{z1}^{(1)} - v_{z2}^{(1)}). \quad (4.13)$$

By checking the inequality, we can determine which case applies to the collision.

Let us consider the specific collision in which the two colliding particles are rolling without sliding. The first particle, which starts with the initial velocities of  $v_{z1}^{(0)} = u_1^{(0)}$  and  $v_{a1}^{(0)} = u_1^{(0)}/s$ , moves toward the second particle, which has velocities of  $v_{z2}^{(0)} = u_2^{(0)}$  and  $v_{a2}^{(0)} = u_2^{(0)}/s$ . Depending on the values of  $u_1^{(0)}$  and  $u_2^{(0)}$ , either Eq. (4.10) or (4.12) can be used to determine the resultant states after the instance of collision. If Eq. (4.13) holds, right after collisions we have

$$\begin{aligned} v_{z1}^{(1)} &= u_2^{(0)}, \\ v_{z2}^{(1)} &= u_1^{(0)}, \\ v_{a1}^{(1)} &= \left(\frac{1}{s} - \mu_{pp}k\right)u_1^{(0)} + \mu_{pp}ku_2^{(0)}, \\ v_{a2}^{(1)} &= (-\mu_{pp}k)u_1^{(0)} + \left(\frac{1}{s} + \mu_{pp}k\right)u_2^{(0)}. \end{aligned} \quad (4.14)$$

After the system evolves into steady state motions, we have

$$v_{z1}^{(2)} = \frac{1}{ks^2+1}(1 - s\mu_{pp}k)u_1^{(0)} + \frac{1}{ks^2+1}(ks^2 + s\mu_{pp}k)u_1^{(0)}, \quad (4.15)$$

$$v_{z2}^{(2)} = \frac{1}{ks^2+1}(ks^2 - s\mu_{pp}k)u_1^{(0)} + \frac{1}{ks^2+1}(1 + s\mu_{pp}k)u_1^{(0)},$$

$$v_{a1}^{(2)} = v_{z1}^{(2)}/s,$$

$$v_{a2}^{(2)} = v_{z2}^{(2)}/s.$$

If Eq. (4.9) does not hold, the relative surface motion between the particles is zero when the two particles are in contact. Right after the collision, we have

$$v_{z1}^{(1)} = u_2^{(0)}$$

$$v_{z2}^{(1)} = u_1^{(0)}$$

$$v_{a1}^{(1)} = \frac{1}{2s}u_1^{(0)} - \frac{1}{2s}u_2^{(0)} \tag{4.16}$$

$$v_{a2}^{(1)} = -\frac{1}{2s}u_1^{(0)} + \frac{1}{2s}u_2^{(0)}$$

After the system evolves into steady state motions, we have

$$v_{z1}^{(2)} = \frac{1}{ks^2+1}(1/2)u_1^{(0)} + \frac{1}{ks^2+1}(ks^2 - 1/2)u_1^{(0)}$$

$$v_{z2}^{(2)} = \frac{1}{ks^2+1}(ks^2 - 1/2)u_1^{(0)} + \frac{1}{ks^2+1}(1/2)u_1^{(0)} \tag{4.17}$$

$$v_{a1}^{(2)} = v_{z1}^{(2)}/s$$

$$v_{a2}^{(2)} = v_{z2}^{(2)}/s$$

The physical meaning of the above derivation is simple: during the collision, the two particles exchange momentum and apply a reciprocal torque, which changes angular momentum; after the collision, the particles accelerate if the translational and angular velocities are mismatched. In both cases, we have  $v_{z1}^{(2)} - v_{z2}^{(2)} = \frac{1-ks^2}{1+ks^2}(v_{z1}^{(0)} - v_{z2}^{(0)})$ , which means that the collision and reacceleration process scale the inter-particle velocity by a factor of  $\frac{1-ks^2}{1+ks^2}$ . If

$$0 < \frac{1-ks^2}{1+ks^2} < 1, \tag{4.18}$$

$n$  secondary collisions after the first impact will occur (with  $n$  going to infinity) because  $v_{z1}^{(2n)} - v_{z2}^{(2n)} > 0$ . For solid spherical particles ( $k = 5/2$ ) on a flat planar surface ( $s = 1$ ), only one collision (i.e., the first impact), is expected to occur. For particles in a v-groove, the condition in Eq. (4.18) implies  $\theta < 78.5^\circ$ , which is satisfied for the specific v-shaped groove that we experimentally fabricated.

In the beginning of the above derivation, we assumed completely elastic collisions between particles. The derivation can be easily generalized to include the case of inelastic collisions, and the prediction of multiple secondary collisions remains valid. For example, if the collision is perfectly inelastic such that both particles obtain the same translational velocity after collision,  $v_{z1}^{(1)} = v_{z2}^{(1)}$ , it follows that  $v_{a1}^{(1)} > v_{a2}^{(1)}$  due to the torque exerted by frictional forces. After the system evolves into steady state, from Eq. (4.3) we have  $v_{z1}^{(2)} - v_{z2}^{(2)} = \frac{s}{ks^2+1} (v_{a1}^{(1)} - v_{a2}^{(1)}) > 0$ , which guarantees another upcoming collision. We can generalize the above derivation for particle-groove systems by adding dissipation that is linearly proportional to the particle velocity. Since the dissipation only scales linearly with the velocity, with a factor of  $\exp\left(-\frac{\Delta t}{T}\right)$ , where  $\Delta t$  is the time difference and  $T$  is the time constant of the dissipation, the system results in a positive final velocity difference:

$$v_{z1}^{(2)} - v_{z2}^{(2)} = \frac{1-ks^2}{1+ks^2} (v_{z1}^{(0)} - v_{z2}^{(0)}) \exp\left(-\frac{\Delta t}{T}\right) > 0. \quad (4.19)$$

In this case, secondary collisions are also expected.

Notice that the criterion of Eq. (4.18) does not depend on the frictional constants of  $\mu_{pp}$  and  $\mu_{pb}$ . This means that the number of expected collisions is independent of the particles' material properties. The presence of multiple secondary collisions can occur in a very large number of systems despite the specific value of Coulomb friction. Such collisions constitute a very universal behavior among various particle-groove systems, including the micro-granular system that we fabricated. In our experimental system,  $\frac{1-ks^2}{1+ks^2} = 0.09$ , and after each collision and reacceleration process the velocity difference,  $(v_{z1}^{(2n+2)} - v_{z2}^{(2n+2)}) = 0.09(v_{z1}^{(2n)} - v_{z2}^{(2n)})$  scales to 9% of its original value. Due to the limited length of the fabricated grooves and limited spatial resolution of the imaging system, the presence of the secondary collisions cannot be resolved in our experiments. However, since the micro-particles are expected to collide multiple times, while they simultaneously lose kinetic

energy via Coulomb friction or other dissipation channels, we can argue that the two particles should end up rolling very close to each other, with  $z_2 - z_1 \sim 2R$ ; this is indeed what we see in the next section.

#### 4.4. Collisions between two particles in a groove

In this section, we experimentally investigate the collisions of two micro-particles in a v-shaped groove and extract the coefficient of restitution for each impact and the frictional constant between the two micro-particles from the measurements (Fig. 4.3). The first micro-particle, which acts as a striker, is positioned in the groove and excited with the laser pulse to reach a maximum velocity of 0.3 m/s before colliding with a stationary micro-particle (i.e., the target particle). Both particles are positioned by a computer-controlled micro-manipulator that has a location accuracy of  $\sim 1 \mu\text{m}$ . We studied two different types of collisions (Fig. 4.2a): (1) collisions that occurred when the striker gained enough angular velocity to roll without sliding before impacting the target particle, and (2) collisions between two micro-particles that are initially positioned in physical contact with each other. In Fig. 4.3b we show a photograph of two micro-particles in a typical experimental run for the first case study. Typical trajectories of micro-particles moving in the groove are shown for the same case in Fig. 4.3c, with the blue line representing the trajectory of the striker particle and the red line that of the target particle. It can be seen that after the collision, the striker particle accelerates due to the Coulomb frictional force. This results from a gain of angular momentum during collision and  $v_z - sv_\alpha < 0$  such that the Coulomb frictional force on the striker is in the positive  $z$  direction. The striker particle quickly catches up with the second particle after the collision, and the two particles keep a distance close to two times their radius, which is what we expected for two particles that are undergoing multiple secondary collisions (see section 4.3 above).

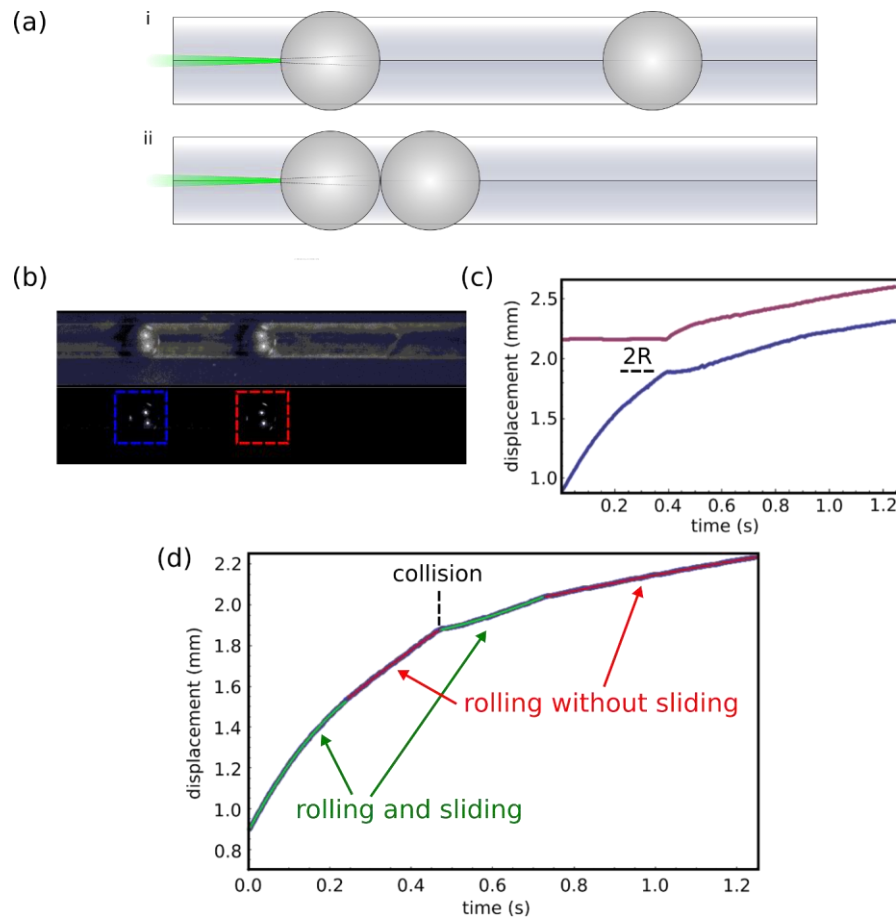


Figure 4.3: Experiments involving particle collisions in a groove. (a) Experimental schematics. Two cases of collisions are tested: a particle collides with another particle that is i) separated by 1 mm, or ii) in direct contact with it. (b) Digital image of the particles during the experiments. The blue and red dashed boxes identify the striker and the target particles, respectively. (c) Trajectories of the two colliding particles. (d) Rolling and sliding motion and rolling without sliding motion as identified for the striker particle. This trajectory reveals information on the angular motion of the particle.

In Fig. 4.3d, we plot the trajectory of the striker particle throughout the collision. The collision point can be clearly identified by the abrupt change in velocity. The particles undergo four ranges of motion, namely rolling and sliding before and after collision (green curves) and rolling without sliding before and after collision (red curves).

We examine the relation of tangential and normal forces between two particles. Throughout this chapter, we have assumed that the tangential force between two particles is well described by Coulomb friction and is linearly proportional to the inter-particle contact force. This is the foundation

of all of our derivations about particle collisions; however, is not true in general [147]. To justify whether it is valid for our system, we examine the ratio between the changes in translational and angular velocities that are caused by collisions.

In order to extract information (i.e., translational and angular velocities) about the particles' motions before and after the collision from the experimental data, we manually separate the trajectory before and after the collision and fit them with the solutions of Eq. (4.5). This allows us to obtain the initial values of  $v_z$  and  $v_a$  and to calculate the values of  $v_z$  and  $v_a$  near the collision. We plot the relation between the change of linear and angular momenta of the target particle (stainless steel 440c) in Fig. 4.4a. We can see that the change of momenta has a linear relationship. Fitting this linear relationship with Eq. (4.9), we obtain the frictional constant between two spheres,  $\mu_{pp}$ , which is equal to 1.4. Despite the large variation in the resulting velocity after collision, the data indicates a linear relationship between inter-particle normal and tangential forces; from an experimental point of view, this can be used to describe our micro-particle system in general.

We are also interested in extracting the coefficient of restitution in the collisions, which is defined as

$$C = \frac{v_{z2}^{(1)} - v_{z1}^{(1)}}{v_{z1}^{(1)} - v_{z2}^{(1)}}, \quad (4.20)$$

This coefficient, which represents the ratio of relative velocities between the two particles before and after collision, is a measure of the efficiency of the collision process. The higher the coefficient of restitution, the more elastic the collision. We plot the experimental coefficients of restitution obtained for the stainless steel micro-particles as a function of the impact velocities in Fig. 4.4b-c; the red squares represent 316, the blue circles 440c. The variations in the values of the experimental coefficient of restitution obtained in our tests are large. Those obtained with stainless steel 316 particles are much larger than those obtained with stainless steel 440c particles, which can be explained by the much rougher surface of the 316 particles (see Chapter 2). Despite the big variation in the measured data, the results show that the coefficient of restitution has velocity dependence and, for both particle types, the coefficient of restitution approaches unity at lower speeds, which means that lower speed collisions are less lossy.

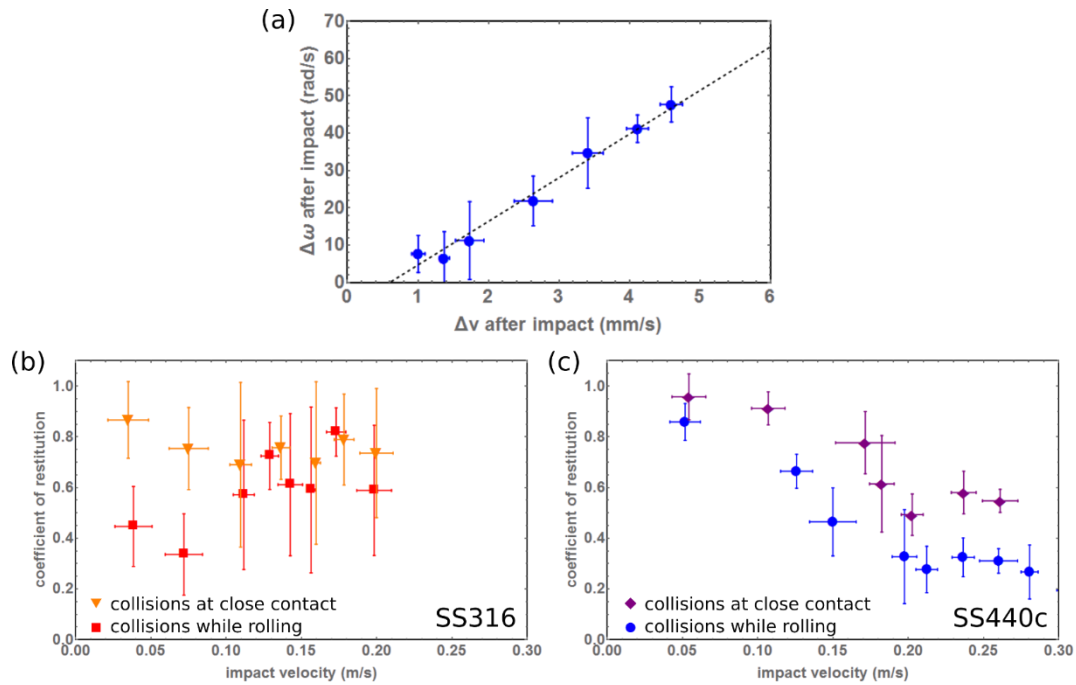


Figure 4.4: Experimental results for the collisions of two particles. (a) A linear correlation between the change of translational and angular velocities during collisions of two 440c particles is observed. The error bars are plotted with  $\pm\sigma/2$ , where  $\sigma$  is the standard deviation of the measurement. Fitting shows the normal force and tangential force can be described with Coulomb friction with a frictional constant of 1.4 (b) The coefficient of restitution between two stainless steel 316 particles when they are rolling (red squares) or initially in contact (orange triangles). (c) The coefficient of restitution between two stainless steel 440c particles when they are rolling (blue circles) or initially in contact (purple diamonds)

We perform measurements to extract the coefficient of restitution for collisions between two particles that are initially in direct contact as well. To create contacting pairs of micro-particles, the computer-controlled micro-manipulator is used to push the two particles together to where the laser beam is focused. The striker particles are excited with varying laser energy and the trajectory of the second particle is measured. Since the striker particle has no trajectory before collision, the initial velocities of the particles are estimated from the calibration of momentum gain at different laser power, as described in Chapter 3. We plot the coefficients of restitution at different impact velocities for both stainless steel 316 (orange triangles) and 440c (purple diamonds) in Fig. 4.4b-c.

The first observations demonstrate that the coefficients of restitution in these measurements are higher than the one measured in the collisions between separated particles, which implies that collisions

result in less loss when the rotational motion of particles is reduced. The coefficient of restitution approaches unity for stainless steel 440c particles, which is again a higher value than the one obtained for the rougher 316 particles. From the calibration results shown in Chapter 3, we know that the momentum gained by the striker has a 15% standard deviation, which should contribute to the error of measurement of the coefficient of restitution. From the data we can see that the standard deviation of the coefficient of restitution for the 440c particles is approximately the same as the contribution of the system; as such we can argue that the resultant velocity after collision should be highly reproducible with uncertainty that is much less than 15%.

These results are fundamentally important to our goal of studying the wave propagation in micro-granular particles, because they imply that neighboring particles in contact can transfer energy with little dissipation within certain ranges of initial velocities. Without this result, the dissipation of the mechanical energy would prevent the propagation of nonlinear waves in a micro-granular chain.

#### 4.5. Summary

In this chapter, we studied the motion and collision of dry micro-particles in a groove and experimentally investigated the fundamental principles that govern their behavior. We modeled the particles in a groove (Eq. (4.8)) with empirical parameters obtained directly from experiments.

$$\frac{d}{dt} v_z = -\text{sign}(v_z - sv_a)g\mu_{pg}/s - \left(\frac{v_z}{T} - \frac{v_z^2}{L}\right),$$

$$\frac{d}{dt} v_a = \text{sign}(v_z - sv_a)kg\mu_{pg},$$

where,  $T = 0.052 \text{ s}$ ,  $L = 2.5 \text{ mm}$ , and  $\mu = 0.337$  and  $0.293$  for stainless steel 316 and 440c, respectively. The empirical model obtained in this chapter was used as the foundation for modeling wave propagation in multi- particle micro-granular systems.

By using proper fitting techniques, we can resolve the angular motion of the particles that are governed by the above equations. After studying the relation between the normal force and tangential force during impact, we found that it can be described with Coulomb friction with  $\mu_{pp} = 1.4$ . We also measured the coefficient of restitution during impact for both separated and neighboring particles. The results show that at low impact velocities, little momentum loss is observed when two micro-particles that are initially in contact collide. This implies the possibility of observing traveling pulses in micro-granular systems that are composed of larger numbers of particles in contact.